AIAA JOURNAL
Vol. 41, No. 1, January 2003

Superelastic and Shape Memory Effects in Laminated Shape-Memory-Alloy Beams

S. Marfia* and E. Sacco†
University of Cassino, 03043 Cassino, Italy
and
J. N. Reddy‡
Texas A&M University, College Station, Texas 77843-3123

A simple shape-memory-alloy (SMA) model to simulate the superelastic behavior as well as the shape memory effect is proposed. It considers only the transformations from austenite to single-variant martensite and from single-variant martensite to austenite, taking into account the influence of the temperature in the constitutive relationship. The proposed SMA constitutive model is employed in a novel layerwise beam theory to develop new SMA beam finite element models with suitable interpolation of the field variables involved. The finite element models developed herein account for the time evolution SMA constitutive equations. In particular, the developed finite elements treat the SMA material as reinforcement of elastic beams. Several applications are presented to assess the validity of the constitutive model and the proposed numerical procedure.

I. Introduction

THE constitutive behavior of shape memory alloys (SMA) presents very special features. In particular, because of the austenite-martensite and martensite-austenite transformations governed by the temperature and the stress state, they can undergo large deformations, exhibiting the so-called superelastic behavior and the shape memory effect. The superelastic behavior occurs when, for a fixed value of the temperature, the material recovers its natural state after a loading-unloading stress cycle. The shape memory effect occurs when an inelastic strain is present after a loading-unloading stress cycle; this inelastic strain can be recovered by a further temperature cycle.

Because of the very special material behavior, SMA materials are successfully employed in many high-tech applications; for example, they are adopted as orthodontic wires, self-expanding microstructures in the treatment of blood vessel occlusions, devices to control the opening of spatial antennas, and in other applications where they are used as sensors and actuators for intelligent composite structures.

Several mathematical models that reproduce the SMA constitutive behavior have been proposed in the last decade. In fact, different micromechanical and macromechanical approaches can be found in the literature in the SMA modeling. The micromechanics-based models were developed using the thermodynamic frame work and micromechanics of a single crystal and evaluating the energies involved during the phase transformations. Moreover, these models adopt homogenization techniques to derive the overall behavior of the SMA.[1−4] On the other hand, the macromechanical models are phenomenological models that are derived considering the overall behavior of the SMA. This approach is useful for engineering applications because of the relative simplicity of implementation in computational procedures. In particular, Boyd and Lagoudas[5,6] proposed a thermodynamically consistent macromechanical model taking into account the phase transformations and the reorientation process in the SMA and considering the stress tensor and temperature as external variables. Auricchio et al.[7] proposed a three-dimensional finite deformations superelastic model within the generalized plasticity framework, developing a suitable numerical procedure. Raniecki and Lexcellent[8] developed a thermodynamic theory able to model the pseudoelastic behavior of SMA introducing a Gibbs potential depending on the temperature and the second and third invariant of the stress deviator. Souza et al.[9] proposed an interesting three-dimensional model considering the strain tensor and the temperature as external variables in which the phase transformations are governed by the second stress invariant. Qidwai and Lagoudas[10] presented a consistent thermodynamical model based on the principal of maximum dissipation transformation considering generalized transformation function (J_2, J_3, I_1 type). The most common structural elements for SMA applications are beams, plates, and shells. Thus, many efforts have been devoted to model and to predict the mechanical response of beams, plates, and shells with SMA imbeddings. Trochu and Qian[11] presented a nonlinear finite element model based on the plasticity theory to study a SMA spring disc. Auricchio and Sacco[12−14] proposed simple and effective one-dimensional thermomechanical models to study the superelastic as well as the shape memory effects for SMA beams. Moreover, they developed finite element formulations and suitable computational procedures. Lagoudas and Shu[15] derived a one-dimensional for SMA wires to study the behavior of a flexible cantilever beam with an externally attached SMA actuator.

In the past few years increased interest has been seen in reinforcing laminated composite beams and plates with wires or layers of shape memory materials. The SMA reinforcements have the following benefits: 1) increase the buckling load significantly and improve the postbuckling behavior[16−18]; 2) reduce deflections and stresses in plates subjected to low-velocity impact[19]; and 3) change the natural frequencies of structures.[20,21]

In the present paper the behavior of SMA laminated beams is investigated. A layered beam structure with two SMA layers in perfect adhesion with the beam core is studied. The kinematic behavior of the composite beam is modeled using the following theories: 1) the Euler–Bernoulli theory, that is, the transverse shear deformation is neglected[22−24]; 2) the Timoshenko theory, that is, the transverse shear deformation is included[22−24]; and 3) a new beam theory, based on the layerwise approach,[25−27] which assumes a constant shear deformation in the beam cross section and neglects the shear deformation in the reinforcement.

The aim of the paper is to model the mechanical response of laminated SMA beams. The constitutive model developed for shape memory alloys is unique in the sense that it accounts for several

Received 19 December 2001; revision received 1 August 2002; accepted for publication 16 August 2002.

*Assistant Professor, Department of Mechanics, Structures and Environment, Via G. Di Biasio, 43; marfia@unicas.it.

†Professor, Department of Mechanics, Structures and Environment, Via G. Di Biasio, 43; sacco@unicas.it.

‡Distinguished Professor, Department of Mechanical Engineering; jnreddy@shakti.tamu.edu. Associate Fellow AIAA.

features of the mechanical behavior in a single model. In particular, a computationally effective one-dimensional SMA constitutive model that is able to reproduce the superelastic behavior as well as the shape memory effect, the martensite reorientation process, the different behavior in tension and in compression of the material, and the different elastic properties of martensite and austenite, is developed. In particular, it considers the transformations from austenite to single-variant martensite and from single-variant martensite to austenite, taking into account the influence of the temperature in the constitutive relationship. The proposed SMA constitutive law is adopted in developing beam finite models that neglect or include the transverse shear deformation. The new SMA beam finite elements are derived, using suitable approximations of the field variables.[27] The finite element models are developed with a numerical procedure for the time integration of the SMA constitutive equations. In particular, the developed finite element models treat the SMA material as reinforcements. Several numerical examples are presented to assess the accuracy of the models. Simulations of interesting advanced applications of SMA devices are also developed.

The paper is organized as follows. Initially a temperature-dependent one-dimensional SMA constitutive law is presented; then, three finite element models based on the Euler–Bernoulli, Timoshenko, and layerwise theories are developed; a computational procedure for the time integration of the time-dependent constitutive equations is described in detail; finally, numerical results of several examples are discussed.

II. Constitutive Model of Shape Memory-Alloy

Shape memory materials can undergo the following phase transformations: 1) from austenite to single-variant martensite, 2) from austenite to multivariant martensite, 3) from single-variant martensite to austenite, 4) from single-variant martensite to multivariant martensite, 5) from multivariant martensite to austenite, and 6) from multivariant martensite to single-variant martensite.

The possible transformations are schematically represented in Fig. 1. The superelastic effect occurs when a loading-unloading process is performed at a temperature greater than T_f^{SA}. The shape memory effect is derived when combinations of temperature and stress paths are performed.

To obtain a simple formulation for modeling the superelastic behavior as well as the shape memory effect, the analysis is restricted

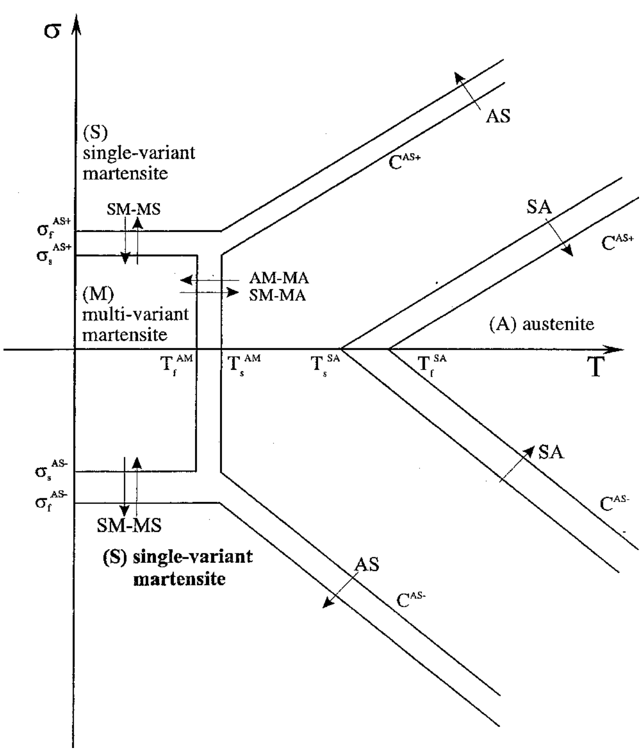

Fig. 1 Scheme of the phase transformations in uniaxial tension and compression vs temperature.

to the case in which the temperature is greater than T_s^{AM}. Thus, only austenite single-variant martensite phase transformations are considered, as schematically illustrated in Fig. 1.

The austenite and the single-variant martensite volume fractions are denoted as ξ_A and ξ_S, respectively. Because it is $\xi_A + \xi_S = 1$,

$$\xi_A = 1 - \xi_S \tag{1}$$

Hence, the single-variant martensite volume fraction is chosen as independent variable governing the phase transformations. Different behavior is considered in tension and in compression. To characterize the response of shape memory alloys, the following material parameters are introduced:

1) E_A and E_S are Young's moduli for the austenite and single-variant martensite, respectively; from the homogenization theory[17] the elastic modulus of the austenite–martensite mixture can be computed as

$$E(\xi_S) = \frac{E_A E_S}{E_S + \xi_S(E_A - E_S)} \tag{2}$$

2) ε_L is the recoverable strain representing a measure of the maximum deformation obtainable aligning all of the single-variant martensites in one direction; it is set as $\varepsilon_L = \varepsilon_L^+$ in tension and $\varepsilon_L = \varepsilon_L^-$ in compression;

3) C^{AS} and C^{SA} are the Clausius–Clapeyron constants for the phase transformations $A \rightarrow S$ and $S \rightarrow A$, respectively; they are set as $C^{AS} = C^{AS,+}$ and $C^{SA} = C^{SA,+}$ in tension and $C^{AS} = C^{AS,-}$ and $C^{SA} = C^{SA,-}$ in compression (Fig. 1);

4) σ_s^{AS} and σ_f^{AS} are the starting and final stress for the $A \rightarrow S$ phase transformation at temperature $T = T_s^{AM}$; they are set as $\sigma_s^{AS} = \sigma_s^{AS,+}$ and $\sigma_f^{AS} = \sigma_f^{AS,+}$ in tension and $\sigma_s^{AS} = \sigma_s^{AS,-}$ and $\sigma_f^{AS} = \sigma_f^{AS,-}$ in compression (Fig. 1).

The process of single-variant martensite production is governed by the evolution equation[13]

$$\dot{\xi}_S = (1 - \xi_S)\mathcal{H}^{AS}\frac{\dot{G}^{AS}}{S_f^{AS} - G^{AS}} \tag{3}$$

where

$$G^{AS} = |\varepsilon| - \frac{C^{AS}}{E}T \tag{4}$$

$$S_f^{AS} = \frac{\sigma_f^{AS} - C^{AS}T_s^{AM}}{E_S} + \varepsilon_L \tag{5}$$

$$S_s^{AS} = \frac{\sigma_s^{AS} - C^{AS}T_s^{AM}}{E} + \varepsilon_L\xi_S \tag{6}$$

$$\mathcal{H}^{AS} = \begin{cases} 1 & \text{when} \quad \begin{cases} \dot{G}^{AS} > 0 \\ S_s^{AS} \le G^{AS} \le S_f^{AS} \end{cases} \\ 0 & \text{otherwise} \end{cases} \tag{7}$$

The process of austenite production is governed by the evolution equation [13]:

$$\dot{\xi}_S = -\xi_S\mathcal{H}^{SA}\frac{\dot{G}^{SA}}{S_f^{SA} - G^{SA}} \tag{8}$$

where

$$G^{SA} = |\varepsilon| - \frac{C^{SA}}{E}T \tag{9}$$

$$S_f^{SA} = \frac{-C^{SA}T_f^{SA}}{E_A} \tag{10}$$

$$S_s^{SA} = \frac{-C^{SA}T_s^{SA}}{E} + \varepsilon_L\xi_S \tag{11}$$

$$\mathcal{H}^{SA} = \begin{cases} 1 & \text{when} \quad \begin{cases} \dot{G}^{SA} < 0 \\ S_f^{SA} \le G^{SA} \le S_s^{SAS} \end{cases} \\ 0 & \text{otherwise} \end{cases} \tag{12}$$

During loading histories, the single-variant martensite undergoes a reorientation process when a transition from tensile to compressive stress or vice versa occurs. To predict this effect, a simple model is proposed. The total strain is obtained as

$$\varepsilon = \varepsilon^e + \xi_S \beta + \alpha(T - T_0) \tag{13}$$

where ε^e is the elastic strain, β is an internal variable describing the change of martensite reorientation, α is the thermal expansion coefficient, and T_0 is the reference temperature. The following evolutive equation is assumed for the parameter β:

$$\dot{\beta} = \begin{cases} \gamma[\varepsilon_L \operatorname{sgn}(\sigma) - \beta][\operatorname{abs}(\sigma) - \sigma^{SS}] & \text{when} \quad \operatorname{abs}(\sigma) > \sigma^{SS} \\ 0 & \text{otherwise} \end{cases} \tag{14}$$

where γ is a material parameter measuring the reorientation process rate and σ^{SS} is a limit stress that activates the reorientation process. Note that σ^{SS} can assume different values in tension, $\sigma^{SS} = \sigma^{SS,+}$, and in compression, $\sigma^{SS} = \sigma^{SS,-}$.

Taking into account Eq. (13), the elastic stress-strain relationship is defined as

$$\sigma = E[\varepsilon - \xi_S \beta - \alpha(T - T_0)] \tag{15}$$

III. Finite Element Models

The SMA material can be used as reinforcements of elastic beams. Thus, in the following the behavior of a reinforced beam made of three different layers is studied: two SMA layers, one on the top and one on the bottom of the elastic beam core.

Three different SMA laminate beam models are developed in the following: the classical Euler–Bernoulli, the Timoshenko, and a new layerwise beam model. The beam length is denoted by L.

A. Euler–Bernoulli Beam Finite Element

First, the Euler–Bernoulli beam finite element model is presented. The kinematics of a laminated SMA beam can be expressed as (Fig. 2a)

$$u_1 = u(x) - z w'(x), \qquad u_3 = w(x) \tag{16}$$

where the prime indicates derivative with respect to x. The only nonzero strain is

$$\varepsilon = \varepsilon_0 + z\kappa \tag{17}$$

where $\varepsilon_0 = u'$ is the axial strain and $\kappa = -w''$ is the curvature. The strain vector is introduced as

$$\boldsymbol{\varepsilon} = \begin{Bmatrix} \varepsilon_0 \\ \kappa \end{Bmatrix} = \begin{Bmatrix} u' \\ -w'' \end{Bmatrix} = \boldsymbol{L} \begin{Bmatrix} u \\ w \end{Bmatrix}, \qquad \boldsymbol{L} = \begin{bmatrix} \dfrac{d}{dx} & 0 \\ 0 & -\dfrac{d^2}{dx^2} \end{bmatrix} \tag{18}$$

The vector of stress resultants is denoted as $\boldsymbol{S} = \{N \quad M\}^T$, where N is the axial force and M the bending moment

$$N = \int_A \sigma \, dA, \qquad M = \int_A z\sigma \, dA \tag{19}$$

Here σ denotes the normal stress and A is the total cross-sectional area of the reinforced beam, that is, the sum of the areas of cross sections of the elastic beam core and the bounding SMA layers.

The nonlinear relations between the kinematic variables and the stress resultants are solved through a numerical procedure. Equations (19) are written in residual form as

$$R_N = \int_A \sigma \, dA - N = 0, \qquad R_M = \int_A z\sigma \, dA - M = 0 \tag{20}$$

Equations (20) are solved using a Newton's algorithm:

$$\begin{Bmatrix} 0 \\ 0 \end{Bmatrix} = \begin{Bmatrix} R_N\left(\varepsilon_0^k, \kappa^k\right) \\ R_M\left(\varepsilon_0^k, \kappa^k\right) \end{Bmatrix} + \boldsymbol{C} \begin{Bmatrix} \varepsilon_0^{k+1} - \varepsilon_0^k \\ \kappa^{k+1} - \kappa^k \end{Bmatrix} \tag{21}$$

where $\boldsymbol{C}$ is the tangent constitutive matrix and the superscripts k and $k+1$ indicate the iteration indices. Given the kth solution, that is, $[\varepsilon_0^k, \kappa^k]$, Eq. (21) can be solved in terms of $(\varepsilon_0^{k+1}, \kappa^{k+1})$. The tangent constitutive matrix is symmetric, and it is obtained performing the derivatives of the residuals:

$$C_{11} = \frac{\partial R_N}{\partial \varepsilon_0} = \int_A \frac{\partial \sigma}{\partial \varepsilon_0} dA, \qquad C_{12} = \frac{\partial R_N}{\partial \kappa} = \int_A \frac{\partial \sigma}{\partial \kappa} dA$$
$$C_{21} = \frac{\partial R_M}{\partial \varepsilon_0} = \int_A z \frac{\partial \sigma}{\partial \varepsilon_0} dA, \qquad C_{22} = \frac{\partial R_M}{\partial \kappa} = \int_A z \frac{\partial \sigma}{\partial \kappa} dA \tag{22}$$

The indicated integration over the beam cross section to determine the residuals and their derivatives is performed analytically for the elastic beam core by discretizing each SMA layer in layers and applying the Gauss integration formulas within each layer.

The finite element formulation is developed introducing suitable approximations of the displacement field (u, w). The axial displacement u is approximated using linear interpolation, whereas the transversal displacement w is interpolated using the Hermite cubic polynomials[28]:

$$\begin{Bmatrix} u \\ w \end{Bmatrix} = \boldsymbol{N}\boldsymbol{U} \tag{23}$$

with

$$\boldsymbol{N} = \begin{bmatrix} N_1^u & 0 & 0 & N_2^u & 0 & 0 \\ 0 & N_1^w & N_1^\theta & 0 & N_2^w & N_2^\theta \end{bmatrix}, \qquad \boldsymbol{U} = \begin{Bmatrix} u_1 \\ w_1 \\ \theta_1 \\ u_2 \\ w_2 \\ \theta_2 \end{Bmatrix} \tag{24}$$

where (u_i, w_i) are the displacement of the ith node and θ_i is the rotation at the i node with $\theta_1 = -w'(0)$ and $\theta_2 = -w'(L)$. The two sets of interpolation functions are

$$N_1^u = (1 - \xi)/2, \qquad N_2^u = (1 + \xi)/2 \tag{25}$$

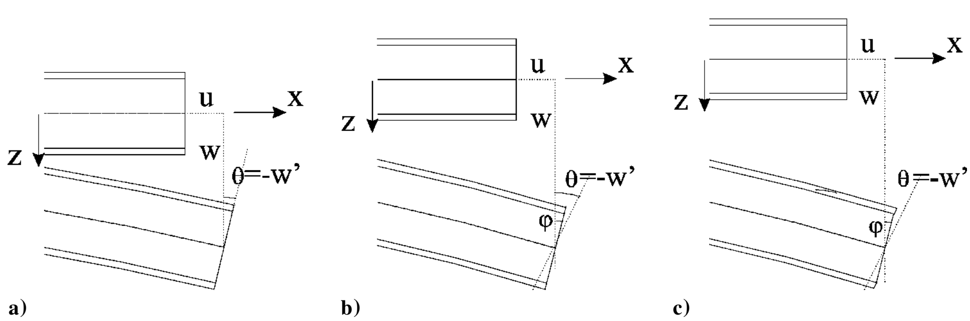

Fig. 2 Kinematics of the a) Euler–Bernoulli, b) Timoshenko, and c) beam models layerwise.

$$N_1^w = (\xi + 2)(\xi - 1)^2/4, \qquad N_1^\theta = -L(\xi + 1)(\xi - 1)^2/8$$
$$N_2^w = -(\xi - 2)(\xi + 1)^2/4, \qquad N_2^\theta = -L(\xi - 1)(\xi + 1)^2/8 \tag{26}$$

where ξ is the normalized local coordinate. The tangent stiffness matrix $\boldsymbol{K}$ of the nonlinear finite element problems is obtained as

$$\boldsymbol{K} = \int_L \boldsymbol{B}^T \boldsymbol{C}\, \boldsymbol{B}\, \mathrm{d}x \tag{27}$$

where $\boldsymbol{B} = \boldsymbol{L}\boldsymbol{N}$.

B. Timoshenko Finite Element

Next, a Timoshenko laminate beam model is developed. It is assumed that the the laminate undergoes a constant state of transverse shear deformation according to the first-order shear deformation theory.[22–24] The kinematics of the Timoshenko beam (see Fig. 2b) can be expressed as

$$u_1 = u(x) + z\varphi(x), \qquad u_3 = w(x) \tag{28}$$

The strain field is given by

$$\varepsilon = \varepsilon_0 + z\kappa, \qquad \gamma = w' + \varphi \tag{29}$$

where $\varepsilon_0 = u'$ is the axial strain, $\kappa = \varphi'$ is the curvature, and γ is the shear strain. The strain vector is

$$\boldsymbol{\varepsilon} = \begin{Bmatrix} \varepsilon_0 \\ \kappa \\ \gamma \end{Bmatrix} = \begin{Bmatrix} u' \\ \varphi' \\ w' + \varphi \end{Bmatrix} = \boldsymbol{L} \begin{Bmatrix} u \\ w \\ \varphi \end{Bmatrix}, \qquad \boldsymbol{L} = \begin{bmatrix} \dfrac{\mathrm{d}}{\mathrm{d}x} & 0 & 0 \\ 0 & 0 & \dfrac{\mathrm{d}}{\mathrm{d}x} \\ 0 & \dfrac{\mathrm{d}}{\mathrm{d}x} & 1 \end{bmatrix} \tag{30}$$

The resultant stress vector is denoted as $\boldsymbol{S} = \{N \;\; M \;\; Q\}^T$, where N is the axial force, M the bending moment, and Q the shear resultant:

$$N = \int_A \sigma\, \mathrm{d}A, \qquad M = \int_A z\sigma\, \mathrm{d}A, \qquad Q = K_s \int_A \tau\, \mathrm{d}A \tag{31}$$

Here, σ and τ are the normal and shear stresses, respectively, whereas K_s is the shear correction factor.

The residual form of Eqs. (31) is

$$R_N = \int_A \sigma\, \mathrm{d}A - N = 0$$
$$R_M = \int_A z\sigma\, \mathrm{d}A - M = 0$$
$$R_Q = \int_A \tau\, \mathrm{d}A - Q = 0 \tag{32}$$

which are solved using a Newton algorithm:

$$\begin{Bmatrix} 0 \\ 0 \\ 0 \end{Bmatrix} = \begin{Bmatrix} R_N\left(\varepsilon_0^k, \kappa^k, \gamma^k\right) \\ R_M\left(\varepsilon_0^k, \kappa^k, \gamma^k\right) \\ R_Q\left(\varepsilon_0^k, \kappa^k, \gamma^k\right) \end{Bmatrix} + \boldsymbol{C} \begin{Bmatrix} \varepsilon_0^{k+1} - \varepsilon_0^k \\ \kappa^{k+1} - \kappa^k \\ \gamma^{k+1} - \gamma^k \end{Bmatrix} \tag{33}$$

The tangent constitutive matrix $\boldsymbol{C}$ is obtained performing the derivatives of the residuals:

$$C_{11} = \frac{\partial R_N}{\partial \varepsilon_0} = \int_A \frac{\partial \sigma}{\partial \varepsilon_0}\, \mathrm{d}A, \qquad C_{12} = \frac{\partial R_N}{\partial \kappa} = \int_A \frac{\partial \sigma}{\partial \kappa}\, \mathrm{d}A$$
$$C_{13} = 0, \qquad C_{21} = \frac{\partial R_M}{\partial \varepsilon_0} = \int_A z\frac{\partial \sigma}{\partial \varepsilon_0}\, \mathrm{d}A$$
$$C_{22} = \frac{\partial R_M}{\partial \kappa} = \int_A z\frac{\partial \sigma}{\partial \kappa}\, \mathrm{d}A, \qquad C_{23} = 0, \qquad C_{31} = 0$$
$$C_{32} = 0, \qquad C_{33} = \frac{\partial R_Q}{\partial \gamma} = \int_A \frac{\partial \tau}{\partial \gamma}\, \mathrm{d}A \tag{34}$$

The integration over the beam cross section is performed numerically to determine the residuals and their derivatives.

The finite element formulation is developed introducing suitable approximations of the generalized displacement field (u, w, φ). The axial displacement u is approximated as linear, whereas the transverse displacement w is interpolated by the Hermite cubic polynomials, and the rotation φ is approximated by quadratic functions[27]:

$$\begin{Bmatrix} u \\ w \\ \varphi \end{Bmatrix} = \boldsymbol{N}\boldsymbol{U} \tag{35}$$

with

$$\boldsymbol{N} = \begin{bmatrix} N_1^u & 0 & 0 & 0 & N_2^u & 0 & 0 & 0 & 0 \\ 0 & N_1^w & N_1^\theta & 0 & 0 & N_2^w & N_2^\theta & 0 & 0 \\ 0 & 0 & 0 & N_1^\varphi & 0 & 0 & 0 & N_2^\varphi & N_3^\varphi \end{bmatrix}, \qquad \boldsymbol{U} = \begin{Bmatrix} u_1 \\ w_1 \\ \theta_1 \\ \varphi_1 \\ u_2 \\ w_2 \\ \theta_2 \\ \varphi_2 \\ \varphi_3 \end{Bmatrix} \tag{36}$$

where u_i, w_i are the displacement of the i node and θ_i represents the Euler–Bernoulli slope at the i node and $\hat{\varphi}_i$ is the actual rotation. The interpolation functions N_i^u, N_i^w, and N_i^θ are reported in formulas (25) and (26), whereas the shape functions N_i^φ are set:

$$N_1^\varphi = \xi[(\xi - 1)/2], \qquad N_2^\varphi = \xi[(\xi + 1)/2], \qquad N_3^\varphi = 1 - \xi^2 \tag{37}$$

The tangent stiffness matrix $\boldsymbol{K}$ is obtained as

$$\boldsymbol{K} = \int_L \boldsymbol{B}^T \boldsymbol{C}\boldsymbol{B}\, \mathrm{d}x \tag{38}$$

where $\boldsymbol{B} = \boldsymbol{L}\boldsymbol{N}$.

The Timoshenko finite element model requires the use of a two-dimensional constitutive equation. On the other hand, for a wide class of beam problems it is reasonable to assume that the values of the normal stresses are generally greater than the values of the shear stresses; moreover, it is apparent that the normal stress influences the phase transformation more significantly than the shear stress. Thus, the one-dimensional SMA constitutive model, proposed in the preceding section, is adopted also for the Timoshenko beam theory, assuming that the phase transformation is governed only by the normal stresses. Moreover, using the same homogenization technique adopted in formula (2) to obtain Young's modulus, one can set the shear modulus as

$$G(\xi_S) = \frac{G_A G_S}{G_S + \xi_S(G_A - G_S)} \tag{39}$$

where G_A and G_S are the shear moduli of the austenite and martensite, respectively.

C. Layerwise Finite Element

A new layerwise beam model is developed for the particular structural problem under investigation. The reinforced beam can be considered made of two different layers: two SMA layers, one on the top and one on the bottom of a beam core. Thus, it is assumed that the two SMA layers do not undergo transverse shear deformations, whereas the core is subjected to a significant shear deformation.

The kinematics of the SMA laminate beam is obtained with reference to Fig. 2c by the expressions[25–27]

$$u_1^R = u^R - zw', \qquad u_1^C = u + z\varphi, \qquad u_3^R = u_3^C = w \tag{40}$$

where the superscripts R and C refer to the reinforcements and to the beam core, respectively. The meanings of the variables u^R and u for the proposed layerwise model are illustrated in Fig. 3. Note that

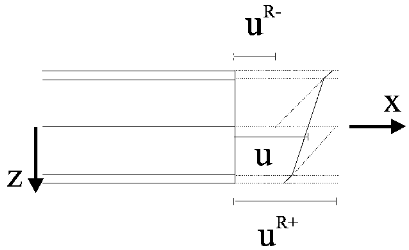

Fig. 3 Layerwise model: u, axial displacement of the core beam; u^{R-}, axial displacement of the reinforcement on the top; and u^{R+}, axial displacement of the reinforcement on the bottom.

$u^R = u^{R-}$ and $u^R = u^{R+}$ represent the axial displacements of the reinforcement on the top and bottom of the beam core, respectevely.

Because of the interface displacement continuity between the beam core and the reinforcement, one has

$$u^R - z_i w' = u + z_i \varphi \Rightarrow u^R = u + z_i(\varphi + w') \tag{41}$$

where z_i indicates the position of the interface of the SMA layer and beam core in the laminate cross section. Thus, the displacement field for the SMA laminated beam is given by

$$u_1^R = u + z_i(\varphi + w') - zw', \qquad u_1^C = u + z\varphi, \qquad u_3^R = u_3^C = w \tag{42}$$

The strain field is computed as

$$\varepsilon^R = \varepsilon_0^R + z\kappa^R, \qquad \gamma^R = 0$$

$$\varepsilon^C = \varepsilon_0^C + z\kappa^C, \qquad \gamma^C = \varphi + w' \tag{43}$$

where $\varepsilon_0^R = u' + z_i(\varphi' + w'')$, $\kappa^R = -w''$, and γ^R are the axial strain, the bending strain, and shear strain of the reinforcement, while $\varepsilon_0^C = u'$, $\kappa^C = \varphi'$, and γ^C have the same meaning for the beam core. The strain vector for the core corresponds to the one computed for the Timoshenko model; on the contrary, the strain of the reinfocement is given by

$$\boldsymbol{\varepsilon}^R = \begin{Bmatrix} \varepsilon_0^R \\ \kappa^R \end{Bmatrix} = \begin{Bmatrix} u' + z_i(\varphi' + w'') \\ -w'' \end{Bmatrix} = \boldsymbol{L}^R \begin{Bmatrix} u \\ w \\ \varphi \end{Bmatrix} \tag{44}$$

where

$$\boldsymbol{L}^R = \begin{bmatrix} \dfrac{\mathrm{d}}{\mathrm{d}x} & z_i \dfrac{\mathrm{d}^2}{\mathrm{d}x^2} & z_i \dfrac{\mathrm{d}}{\mathrm{d}x} \\ 0 & \dfrac{\mathrm{d}^2}{\mathrm{d}x^2} & 0 \end{bmatrix} \tag{45}$$

The layerwise beam model is obtained assembling the equations of the Euler–Bernoulli theory for the reinforcement and the Timoshenko theory for the core. The governing equations for the core correspond to the one obtained in the preceding subsection adopting a linear constitutive law.

Equation (20) represents the governing equation for the reinforcement when the integral is performed on the area of the reinforcement A_R, that is, when it is set $A = A_R$. The tangent constitutive matrix for the reinforcement is given by Eq. (22).

The displacement field (u, w, φ) is approximated by Eqs. (35) and (36), where the interpolation functions (25), (26), and (37) are considered for the axial displacement u, the transversal displacement w, and the rotation φ, respectively. The tangent stiffness matrix of the layerwise finite element is obtained assembling the linear elastic Timoshenko stiffness matrix with the tangent stiffness matrix of the reinforcement obtained by formula (27) with $\boldsymbol{B} = \boldsymbol{L}^R\boldsymbol{N}$ with $\boldsymbol{N}$ specified in Eq. (36).

It should be emphasized that, according the proposed layerwise theory, the one-dimensional SMA constitutive equation is required in the reinforcement layers. Thus, contrarly to the Timoshenko finite element presented in the previous subsection, it is not necessary to introduce approximations on the shear behavior of the SMA material, but the one-dimensional constitutive model detailed in Sec. II is consistently applied.

IV. Time-Integration Procedure

The evolution equations governing the SMA phase transformations introduced in the preceding section are solved developing a step-by-step time-integration algorithm. In particular, once the solution at the time t_n is determined, the solution at the current time $t_{n+1} = t_n + \Delta t$ is evaluated adopting a backward-Euler implicit integration procedure.[29,30] In the following, the quantities with the subscript n are related to the preceding time step t_n, whereas the ones with no subscript are referred to the current step t_{n+1}.

The discretized form of the evolution equations (3) and (8) is

$$R_1 = \lambda_S\left(G^{AS} - S_f^{AS}\right) + (1 - \xi_S)\left(G^{AS} - G_n^{AS}\right)\mathcal{H}^{AS} = 0 \tag{46}$$

$$R_2 = \lambda_S\left(G^{SA} - S_f^{SA}\right) - \xi_S\left(G^{SA} - G_n^{SA}\right)\mathcal{H}^{SA} = 0 \tag{47}$$

where

$$\lambda_S = \int_{t_n}^{t_{n+1}} \dot{\xi}_S \,\mathrm{d}t \tag{48}$$

$$\xi_S = \xi_{S,n} + \lambda_S \tag{49}$$

Note that the phase transformations austenite–martensite and martensite–austenite cannot occur at the same time. Thus, when $\mathcal{H}^{AS} = 1$ then $\mathcal{H}^{SA} = 0$ and, on the contrary, when $\mathcal{H}^{SA} = 1$ then $\mathcal{H}^{AS} = 0$. As a consequence, during the phase transformation only one of the two residual equations (46) and (47) is not trivial and has to be solved.

For $\mathcal{H}^{AS} = 1$ substitute Eqs. (49) and (4) into Eq. (46) and take into account the formula (2) giving the Young modulus E, one obtains

$$0 = \lambda_S\left(-S_f^{AS} + G_n^{AS}\right) - (1 - \xi_{S,n})G_n^{AS} + (1 - \xi_{S,n})$$
$$\times\left\{|\varepsilon| - [E_S + (\xi_{S,n} + \lambda_S)(E_A - E_S)]\left(C^{AS}\big/E_A E_S\right)T\right\}$$

which gives the expression for the single-variant martensite increment during the finite step Δt:

$$\lambda_S = \frac{(1 - \xi_{S,n})\left\{|\varepsilon| - [E_S + \xi_{S,n}(E_A - E_S)]\left(C^{AS}\big/E_A E_S\right)T - G_n^{AS}\right\}}{\left(S_f^{AS} - G_n^{AS}\right) + (1 - \xi_{S,n})(E_A - E_S)\left(C^{AS}\big/E_A E_S\right)T} \tag{50}$$

Following the same procedure for $\mathcal{H}^{SA} = 1$, that is, substituting formulas (49), (9), and (2) into Eq. (47), results in

$$0 = \lambda_S\left(-S_f^{SA} + G_n^{SA}\right) - \xi_{S,n}\left\{|\varepsilon| - [E_S\right.$$
$$\left. + (\xi_{S,n} + \lambda_S)(E_A - E_S)]\left(C^{SA}/E_A E_S\right)T - G_n^{SA}\right\} \tag{51}$$

which gives

$$\lambda_S = \frac{-\xi_{S,n}\left\{|\varepsilon| - [E_S + \xi_{S,n}(E_A - E_S)]\left(C^{SA}\big/E_A E_S\right)T - G_n^{SA}\right\}}{\left(S_f^{SA} - G_n^{SA}\right) - \xi_{S,n}(E_A - E_S)\left(C^{SA}\big/E_A E_S\right)T} \tag{52}$$

The time integration of the evolution equation (14) of the reorientation parameter β when it occurs, that is, when $\mathrm{abs}(\sigma) > \sigma^{SS}$, gives

$$\beta = \beta_n + \begin{cases} \Delta t\gamma(\varepsilon_L - \beta)(\sigma - \sigma^{SS}) & \text{when} \quad \sigma > \sigma^{SS} \\ \Delta t\gamma(\varepsilon_L + \beta)(\sigma + \sigma^{SS}) & \text{when} \quad \sigma < -\sigma^{SS} \end{cases} \tag{53}$$

Substituting the expression of σ given by formula (15) into Eq. (53) yields

$$a\beta^2 + b\beta + c = 0 \tag{54}$$

The coefficients of the second-order equation (54) are as follows:

For $\sigma > \sigma^{SS}$:

$$a = E\xi_S \Delta t\gamma$$
$$b = -1 - \Delta t\gamma E[\varepsilon - \alpha(T - T_0)] - \Delta t\gamma\varepsilon_L E\xi_S + \Delta t\gamma\sigma^{SS}$$
$$c = -\Delta t\gamma\varepsilon_L\sigma^{SS} + \beta_n + \Delta t\gamma\varepsilon_L E[\varepsilon - \alpha(T - T_0)] \quad (55)$$

For $\sigma < -\sigma^{SS}$:

$$a = -E\xi_S \Delta t\gamma$$
$$b = -1 + \Delta t\gamma E[\varepsilon - \alpha(T - T_0)] - \Delta t\gamma\varepsilon_L E\xi_S + \Delta t\gamma\sigma^{SS}$$
$$c = \Delta t\gamma\varepsilon_L\sigma^{SS} + \beta_n + \Delta t\gamma\varepsilon_L E[\varepsilon - \alpha(T - T_0)] \quad (56)$$

The differentiation of the constitutive equation (15) gives

$$\mathrm{d}\sigma = \{E^* A[\varepsilon - \xi_S\beta - \alpha(T - T_0)] + E(1 - A\beta - B\xi_S)\}\,\mathrm{d}\varepsilon \quad (57)$$

where

$$E^* = \frac{\partial E}{\partial \xi_S}, \qquad A = \frac{\partial \xi_S}{\partial \varepsilon} = \frac{\partial \lambda_S}{\partial \varepsilon}, \qquad B = \frac{\partial \beta}{\partial \varepsilon} \quad (58)$$

In particular, one has

$$E^* = \frac{\partial E}{\partial \xi_S} = -E^2 \frac{E_A - E_S}{E_A E_S} \quad (59)$$

$$A = \frac{(1 - \xi_{S,n})\,\mathrm{sgn}(\varepsilon)}{\left(S_f^{AS} - G_n^{AS}\right) + (1 - \xi_{S,n})(E_A - E_S)\left(C^{AS}/E_A E_S\right)T}$$
$$\text{if} \quad \mathcal{H}^{AS} = 1 \quad (60)$$

$$A = \frac{-\xi_{S,n}\,\mathrm{sgn}(\varepsilon)}{\left(S_f^{SA} - G_n^{SA}\right) - \xi_{S,n}(E_A - E_S)\left(C^{SA}/E_A E_S\right)T}$$
$$\text{if} \quad \mathcal{H}^{SA} = 1 \quad (61)$$

$$B = \frac{E^* A[\varepsilon - \xi_S\beta - \alpha(T - T_0)] + E(1 - A\beta)}{[1 + \Delta t\,\gamma(\sigma - \sigma^{SS})/\Delta t\gamma(\varepsilon_L - \beta)] + E\xi_S}$$
$$\text{if} \quad \sigma > \sigma^{SS} \quad (62)$$

$$B = \frac{E^* A[\varepsilon - \xi_S\beta - \alpha(T - T_0)] + E(1 - A\beta)}{[1 - \Delta t\,\gamma(\sigma + \sigma^{SS})/\Delta t\gamma(\varepsilon_L + \beta)] + E\xi_S}$$
$$\text{if} \quad \sigma \le \sigma^{SS} \quad (63)$$

V. Numerical Results

In this section numerical results obtained using the Euler–Bernoulli, Timoshenko, and layerwise SMA finite elements are presented. Initially, comparisons with three-dimensional analytical solutions are presented. Then, interesting applications of SMA laminates are presented to discuss the superelastic and the shape memory effects.

A. Comparisons with Three-Dimensional Analytical Solution

Consider a simply supported beam subjected to a sinusoidal distributed transverse load. The beam is characterized by a rectangular cross section with an elastic core and elastic reinforcements on the top and bottom. Two different materials are adopted for the core and for the reinforcements. The geometric and material nondimensional parameters are

$$b/L = 1, \qquad h/L = 0.08 \sim 0.26, \qquad h_R/h = \rho$$
$$E_R/E_C = 25, \qquad G_R/E_C = 0.5, \qquad G_C/E_C = 0.2 \quad (64)$$

where b, h, and h_R are the thickness, the height of the cross section, and the height of each reinforcement, respectively; L is the length of the beam; and E_R, E_C and G_R, G_C are the Young's and shear moduli for the reinforcements and for the core, respectively. The analysis is carried out for two different values of the ratio $\rho = \frac{1}{6}$ and $\rho = \frac{1}{4}$.

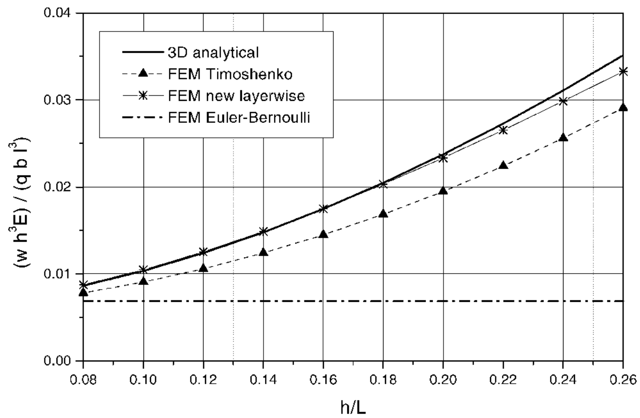

a)

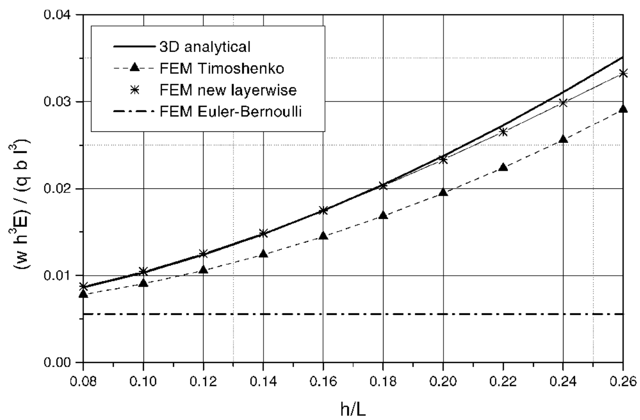

b)

Fig. 4 Analytical three-dimensional solution vs Timoshenko and layerwise finite element model solutions for a) $\rho = \frac{1}{6}$ and b) $\rho = \frac{1}{4}$.

The numerical results obtained by the three laminate models discussed herein are compared with the three-dimensional analytical solution. Computations are developed adopting a uniform mesh of 10 elements. In Fig. 4 the nondimensional maximum traverse displacement $w_{\max} = wh^3E/(qbL^3)$ vs h/L is plotted for $\rho = \frac{1}{6}$ and $\frac{1}{4}$. From Fig. 4 it can be noted that the results obtained with the newly developed layerwise model are very satisfactory because they are able to approximate the three-dimensional analytical solution more accurately than the Euler–Bernoulli or the Timoshenko models.

B. SMA Laminate Data

In the examples discussed next, the behavior of cantilever beams reinforced by SMA layers on the bottom and top is investigated. The material properties of the SMA reinforcements are as follows:

$$E_A = 47{,}000\ \text{MPa}, \qquad E_S = 17{,}000\ \text{MPa}, \qquad \varepsilon_L^+ = 0.08$$
$$\varepsilon_L^- = 0.06, \qquad G_A = 20{,}000\ \text{MPa}, \qquad G_S = 8000\ \text{MPa}$$
$$T_s^{AM} = 10^\circ\text{C}, \qquad T_f^{AM} = 5^\circ\text{C}, \qquad T_s^{SA} = 30^\circ\text{C}$$
$$T_f^{SA} = 31^\circ\text{C}, \qquad \sigma_s^{AS,-} = 196\ \text{MPa}, \qquad \sigma_f^{AS,-} = 196\ \text{MPa}$$
$$\sigma_s^{AS,+} = 140\ \text{MPa}, \qquad \sigma_f^{AS,+} = 141\ \text{MPa}$$
$$C^{AS,+} = 6\ \text{MPa}/^\circ\text{C}, \qquad C^{AS,-} = 8.6\ \text{MPa}/^\circ\text{C}$$
$$C^{SA,+} = 8\ \text{MPa}/^\circ\text{C}, \qquad C^{SA,-} = 11.2\ MPa/^\circ\text{C}$$
$$\sigma^{SS,+} = 30\ \text{MPa}, \qquad \sigma^{SS,-} = 40\ \text{MPa}, \qquad \alpha = 0.00002 \quad (65)$$

These values correspond to the Ni-Ti alloys produced by GAC International, Inc., and tested by Airoldi et al.[31]

The material properties of the elastic beam core are

$$E_c = 10{,}000\ \text{MPa}, \qquad G_c = 4000\ \text{MPa}, \qquad \alpha_c = 0.00005 \quad (66)$$

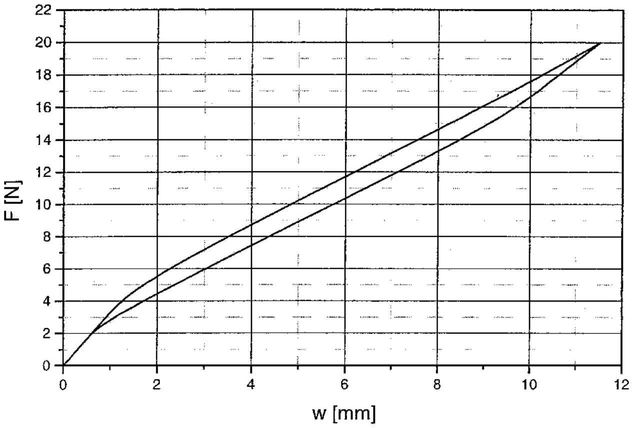

Fig. 5 Superelastic behavior of the SMA laminated cantilever beam: applied force vs transversal displacement at the free-end cross section.

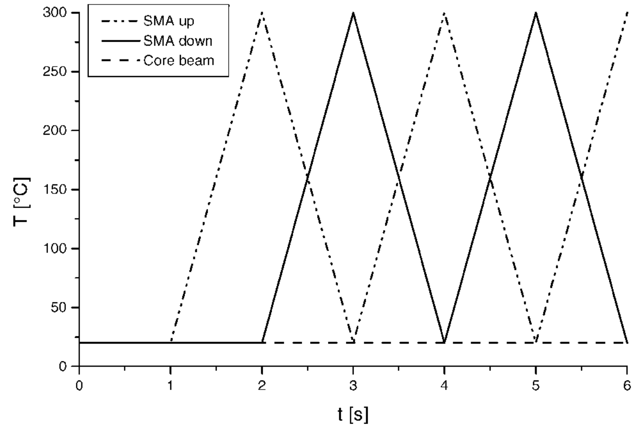

Fig. 6 Temperature cycles for the SMA layers applied on the top and the bottom of the core beam.

Moreover, it is assumed that reinforced cantilever beam has a rectangular cross section with

$$L = 12 \text{ mm}, \qquad b = 1 \text{ mm} \tag{67}$$

where L is the length and b is the width of the rectangular cross section.

C. Superelastic Behavior

Initially, the superelastic behavior of a beam subjected to a point load F acting at the free end is investigated. The beam and reinforcements thicknesses are taken to be

$$h = 1 \text{ mm}, \qquad h_R = 0.05 \text{ mm} \tag{68}$$

A loading-unloading history under constant reference temperature $T_0 = 60°\text{C}$ is considered.

Numerical results are obtained using the SMA beam finite element based on the Euler–Bernoulli theory, considering a mesh of three elements. In Fig. 5 the mechanical response of the reinforced beam is plotted in terms of the concentrated force F vs the tranverse displacement w of the free end of the beam. The typical hysteretic behavior of the superelastic effect of the SMA reinforcements can be exploited to damp out vibrations.

D. SMA Actuator

An interesting application of the SMA laminate is presented next. In fact, the shape memory effect of the Ni-Ti layers is used to design a cantilever beam, characterized by the material and geometry data (65), (66), (67), and (68), as an SMA actuator.

The objective is to govern the transverse displacement of the cantilever beam performing temperature changes in the SMA layers. To obtain phase transformation by temperature variations, the SMA layers have to be prestressed in tension. To this end, the elastic core is initially subjected to a precompression by applying an axial displacement δ. In particular, three different prescribed axial displacements are considered in the computations: $\delta = 1.80$, 1.20, and 0.84 mm.

After the core precompression the SMA reinforcements are perfectly glued on the top and bottom of the beam. The laminate is not loaded by external mechanical forces, but the two SMA layers are subjected to the temperature history represented in Fig. 6. The reference temperature is taken to be $T_0 = 20°\text{C}$. Different cycles of temperature are considered for the upper and lower SMA reinforcements. Because no external forces are applied on the cantilever, the shear force is zero during the whole temperature history; therefore, shear deformation is zero in the beam, which can be satisfactory modeled using the Euler–Bernoulli element. In particular, a mesh of only one element is considered in the computations.

In Fig. 7 the axial and the transversal displacements of the free end vs time is reported for the three different values of the prescribed axial displacements δ. Although the axial displacement is constant during the temperature cycles, the transverse displacement

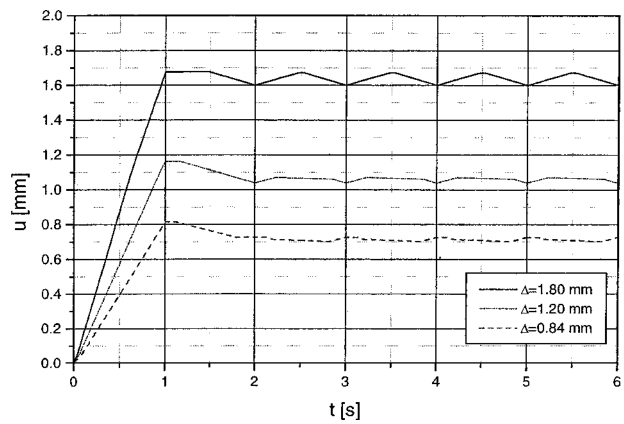

a) Axial

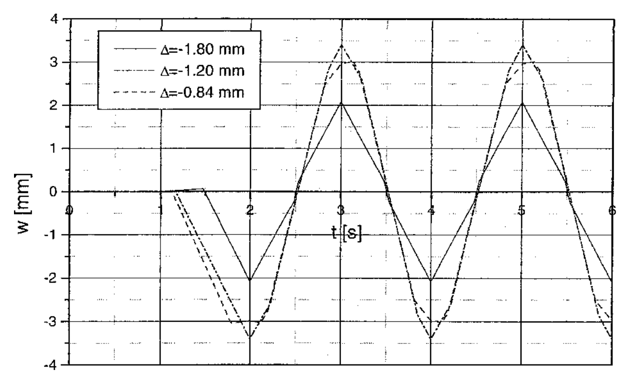

b) Transversal

Fig. 7 Displacement of the free-end cross section vs time for the actuator controlled by the temperature of the SMA layers on the top and on the bottom of the core beam.

undergoes remarkable variations. In fact, the changes in temperature induce significant variation of the laminate deflection. Thus, the structure represents an accurate actuator with fine and simple temperature control. Figure 7 also shows the significant dependence of the cantilever response on the prescribed axial displacements δ; in particular, it can be pointed out that, by increasing the value of δ, the transverse displacements decrease.

E. SMA Actuator with External Force

The actuator proposed in the preceding subsection is reconsidered. Now, the presence of a concentrated force $F(t) = F_{\max} g(t)$ acting on the free end is assumed. The actual variation of $g(t)$ with time t is shown in Fig. 8. Results are obtained assuming a prescribed precompression $\delta = 0.84$ mm, whereas three different values are considered for the maximum value of the external force: $F_{\max} = 25$ N,

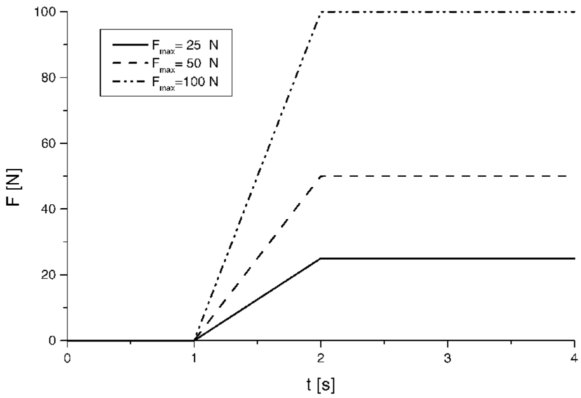

a)

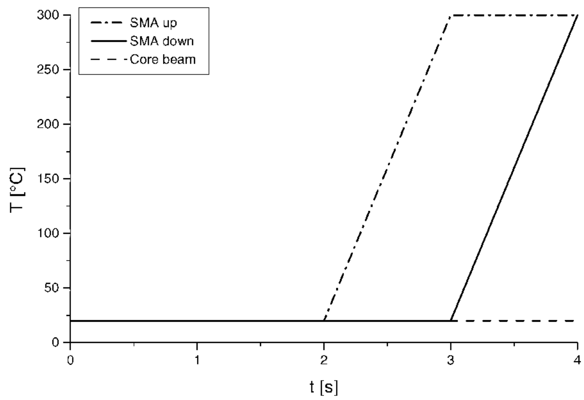

b)

Fig. 8 Loading history of the concentrated force *F* at the free end and temperature *T* in the SMA layers and beam core for the shear deformable actuator.

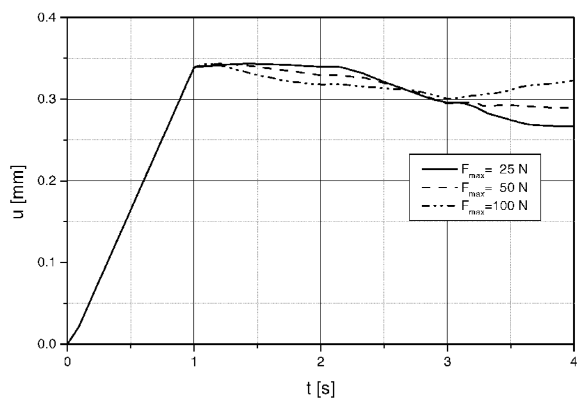

a) Axial

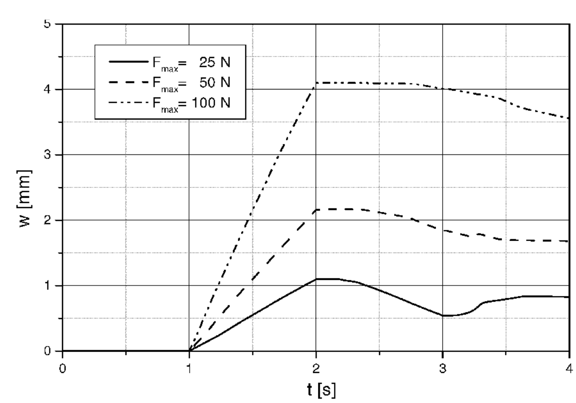

b) Transversal

Fig. 9 Displacement of the free-end cross section vs time for the actuator loaded by a concentrated force and controlled by the temperature of the SMA layers on the top and on the bottom of the core beam.

$F_{max} = 50$ N, and $F_{max} = 100$ N. In particular, the loading history in terms of applied force F and temperature T on the top and bottom SMA layers is shown in Fig. 8.

Because of the presence of the external force F, the shear force is not zero, and the shear deformation in the thickness direction is not negligible. The layerwise finite element model is most suitable for this case. A mesh of three elements is used.

In Fig. 9a the axial displacement of the cantilever end section vs time is plotted. Negligible variations of axial displacement are noted for three different values of the external force F. Figure 9b contains plots of the transverse displacement of the free end vs time. The influence of F_{max} on the mechanical response is clear. Moreover, the transverse displacement can be controlled by temperature changes. In particular, for $F_{max} = 25$ N the 50% of the total transverse displacement is recovered, heating the SMA layer at the top of the beam.

F. Shape Memory Effect

As a final example, a comparison of the shape memory effect predicted by the three beam finite elements is presented. The cross section of the beam is constituted by an elastic core and two SMA reinforcements, one on the top and the other on the bottom of the beam. The geometric data used are

$$h = 3\ \text{mm}, \qquad h_R = 0.75\ \text{mm} \tag{69}$$

The cantilever beam, modeled adopting the three finite element models, is subjected to the following loading history in terms of

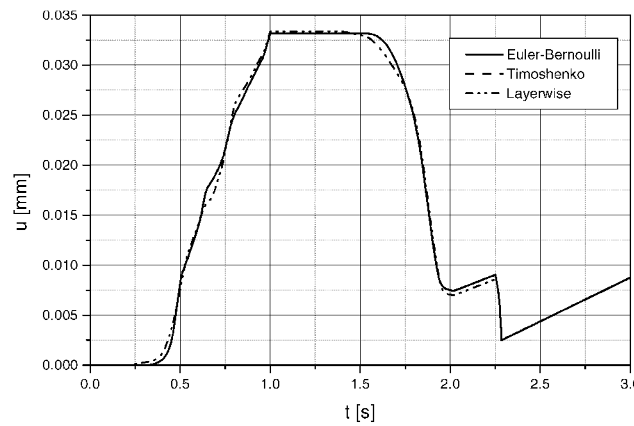

a)

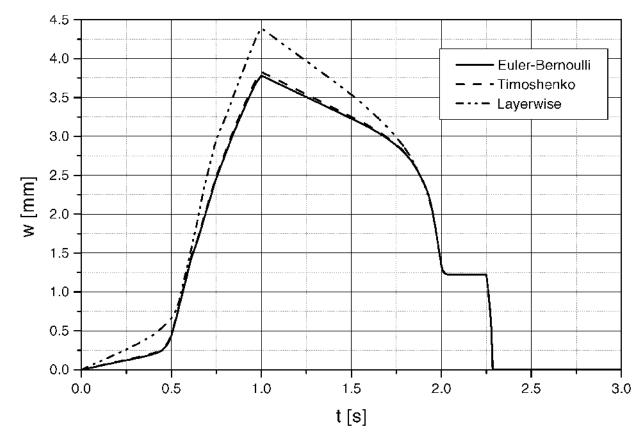

b)

Fig. 10 a) Axial displacement and b) transversal displacement of the free end cross section vs time for the SMA laminate loaded by a concentrated force and controlled by the temperature; comparison of the three finite elements.

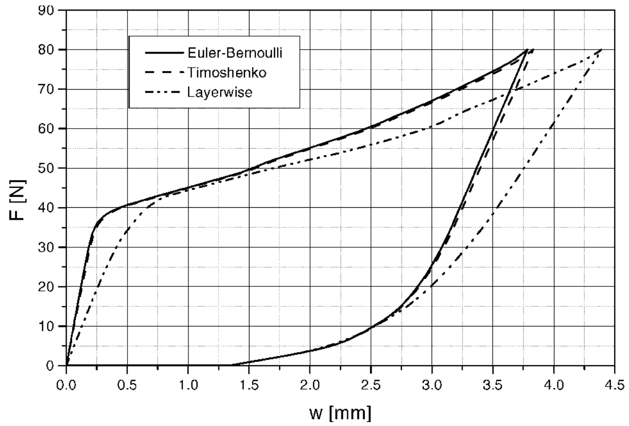

Fig. 11 Shape-memory effect for the SMA laminate evaluated by the three proposed finite element models.

concentrated force F applied at the free end and temperature of the beam:

$$
\begin{aligned}
t &= 0\ \mathrm{s}, \qquad F = 0\ \mathrm{N}, \qquad T = 20^\circ\mathrm{C}\\
t &= 1\ \mathrm{s}, \qquad F = 20\ \mathrm{N}, \qquad T = 20^\circ\mathrm{C}\\
t &= 2\ \mathrm{s}, \qquad F = 0\ \mathrm{N}, \qquad T = 20^\circ\mathrm{C}\\
t &= 3\ \mathrm{s}, \qquad F = 0\ \mathrm{N}, \qquad T = 60^\circ\mathrm{C}
\end{aligned}
\tag{70}
$$

Linear variations of the force and temperature are assumed within each time step.

In Fig. 10a, a plot of the axial displacement of the end vs time is shown. It is observed that there is very little difference among the predictions of the Euler–Bernoulli, Timoshenko, and layerwise models. The difference is more evident in terms of transverse displacement vs time, shown in Fig. 10b, and in terms of force vs transverse displacement, shown in Fig. 11, which represents the overall mechanical response of the beam. It can be noted from Fig. 11 that the mechanical response of the beam is strongly influenced by the shape memory effect of the SMA reinforcements.

VI. Conclusions

A simple and effective SMA model is proposed. It is able to reproduce the superelastic as well as the shape memory effect. Three laminate finite element models based on three different beam theories are developed. In particular, the layerwise beam model developed herein is novel, and it is characterized by the same degrees of freedom as the Timoshenko beam element. A numerical procedure is also developed for the integration of the SMA evolution equations. The performance of the three models is investigated with a number of problems. Results show very satisfactory behavior of the layerwise finite element over the other models. Superlasticity and shape memory effects were also investigated in the numerical applications.

The constitutive as well kinematic models developed herein can possibly be used to design simple and effective actuators. The study demonstrates the sensitivity of the transverse displacement from the temperature of the SMA layers. Moreover, it is shown that SMA actuators are very effective because they are able to produce large amounts of work; in fact, it is possible to recover as much as 50% of the displacement as a result of the application of external forces by performing temperature cycles on the SMA layers.

Acknowledgments

The first two authors gratefully acknowledge the financial supports of the Italian National Research Council and of the Ministry of University and Research. The third author acknowledges the support of this research by U. S. Army Research Office Grant DAAD 19-01-1-0483. Thanks are also given to F. Auricchio, University of Pavia, for the the useful discussions in the SMA modeling.

References

[1]Patoor, E., Eberhardt, A., and Berveille, M., "Thermomechanical Behavior of Shape Memory Alloys," *Archives of Mechanics*, Vol. 40, Nos. 5 and 6, 1988, pp. 775–794.

[2]Goo, B. C., and Lexcellent, C., "Micromechanics-Based Modeling of Two-Way Memory Effect of a Single Crystalline Shape-Memory Alloy," *Acta Materialia*, Vol. 45, No. 2, 1997, pp. 727–737.

[3]Huang, M., and Brinson, L. C., "A Multivariant Model for Single Crystal Shape Memory Alloy Behavior," *Journal of the Mechanics and Physics of Solids*, Vol. 46, No. 8, 1998, pp. 1379–1409.

[4]Siderey, N., Patoor, E., Berveiller, M., and Eberhardt, A., "Constitutive Equations for Polycystalline Thermoelastic Shape Memory Alloys. Part I. Intragranular Interactions and Behavior of the Grain," *International Journal of Solids and Structures*, Vol. 36, No. 8, 1999, pp. 4289–4315.

[5]Boyd, J. G., and Lagoudas, D. C., "Thermomechanical Response of Shape Memory Composites," *Journal of Intelligent Materials Systems and Structures*, Vol. 5, No. 3, 1994, pp. 333–346.

[6]Boyd, J. G., and Lagoudas, D. C., "A Thermodynamic Constitutive Model for Shape Memory Materials. Part I: The Monolithic Shape Memory Alloys," *International Journal of Plasticity*, Vol. 12, No. 6, 1995, pp. 805–841.

[7]Auricchio, F., Taylor, R. L., and Lubliner, J., "Shape-Memory Alloys: Macromodelling and Numerical Simulations of Superelastic Behavior," *Computer Methods in Applied Mechanics and Engineering*, Vol. 146, Nos. 3–4, 1997, pp. 281–312.

[8]Raniecki, B., and Lexcellent, Ch., "Thermodynamics of Isotropic Pseudoelasticity in Shape-Memory Alloys," *European Journal of Mechanics—A/Solids*, Vol. 17, No. 2, 1998, pp. 185–205.

[9]Souza, A., Mamiya, E., and Zouain, N., "Three-Dimensional Model for Solids Undergoing Stress-Induced Phase Transformation," *European Journal of Mechanics—A/Solids*, Vol. 17, No. 5, 1998, pp. 789–806.

[10]Qidwai, M. A., and Lagoudas, D. C., "On Thermomechanics and Trasformation Surfaces of Polycrystalline NiTi Shape Memory Alloy Material," *International Journal of Plasticity*, Vol. 16, Nos. 10–11, 2000, pp. 1309–1343.

[11]Trochu, F., and Qian, Y. Y., "Nonlinear Finite Element Simulation of Superelastic Shape Memory Alloy Parts," *Computers and Structures*, Vol. 62, No. 5, 1997, pp. 799–810.

[12]Auricchio, F., and Sacco, E., "A Superelastic Shape-Memory-Alloy Beam Model," *Journal of Intelligent Materials Systems and Structures*, Vol. 8, No. 6, 1997, pp. 489–501.

[13]Auricchio, F., and Sacco, E., "A Temperature-Dependent Beam for Shape-Memory Alloys: Constitutive Modelling, Finite-Element Implementation and Numerical Simulations," *Computer Methods in Applied Mechanics and Engineering*, Vol. 174, Nos. 1–2, 1999, pp. 171–190.

[14]Auricchio, F., and Sacco, E., "Thermo-Mechanical Modelling of a Superelastic Shape-Memory Wire under Cyclic Stretching-Bending Loadings," *International Journal of Solids and Structures*, Vol. 38, Nos. 34–35, 2001, pp. 6123–6145.

[15]Lagoudas, D. C., and Shu, S. G., "Residual Deformation of Active Structures with SMA Actuators," *International Journal of Mechanical Science*, Vol. 41, No. 6, 1999, pp. 595–619.

[16]Birman, V., "Theory and Comparison of the Effect of Composite and Shape Memory Alloy Stiffeners on Stability of Composite Shells and Plates," *International Journal of Mechanical Sciences*, Vol. 39, No. 10, 1997, pp. 1139–1149.

[17]Lee, J. J., and Choi, S., "Thermal Buckling and Postbuckling Analysis of a Laminated Composite Beam with Embedded SMA Actuators," *Composite Structures*, Vol. 47, Nos. 1–4, 1999, pp. 695–703.

[18]Thompson, S. P., and Loughlan, J., "The Control of the Post-Buckling Response in Thin Plates Using Smart Technology," *Thin-Walled Structures*, Vol. 36, No. 4, 2000, pp. 231–263.

[19]Birman, V., Chandrashekhara, K., and Sain, S., "An Approach to Optimization of Shape Memory Alloy Hybrid Composite Plates Subjected to Low-Velocity Impact," *Composites: Part B*, Vol. 27B, No. 5, 1996, pp. 439–446.

[20]Chen, Q., and Levy, C., "Vibration Analysis and Control of Flexible Beam by Using Smart Damping Structures," *Composites: Part B*, Vol. 30, No. 4, 1999, pp. 395–406.

[21]Ostachowicz, W., Krawczuk, M., and Żak, A., "Dynamics and Buckling of a Multilayer Composite Plate with Embedded SMA Wires," *Composite Structures*, Vol. 48, Nos. 1–3, 2000, pp. 163–167.

[22]Reddy, J. N., *Theory and Analysis of Elastic Plates*, Taylor and Francis, Philadelphia, PA, 1999.

[23]Wang, C. M., Reddy, J. N., and Lee, K. H., *Shear Deformable Beams and Plates. Relationship with Classical Solutions*, Elsevier, Oxford, 2000.

[24]Reddy, J. N., *Energy Principles and Variational Methods in Applied Mechanics*, Wiley, New York, 2002.

[25]Reddy, J. N., "A Generalization of Two-Dimensional Theories of Laminated Plates," *Communications in Numerical Methods in Engineering*, Vol. 3, No. 3, 1987, pp. 173–180.

[26]Reddy, J. N., *Mechanics of Laminated Composite Plates. Theory and Analysis*, CRC Press, Boca Raton, FL, 1997.

[27]Marfia, S., Sacco, E., and Reddy, J. N., "A New Locking-Free Timoshenko Beam Finite Element," *Journal of Engineering Mechanics* (submitted for publication).

[28]Reddy, J. N., *An Introduction to the Finite Element Method*, 2nd ed., McGraw–Hill, New York, 1993.

[29]Crisfield, M. A., *Non-Linear Finite Element Analysis of Solids and Structures*, Vol. 1, Wiley, New York, 1991.

[30]Simo, J. C., and Hughes, T. J. R., *Computational Inelasticity*, Springer-Verlag, New York, 1998.

[31]Airoldi, G., Riva, G., and Vannelli, M., "Superelasticity and Shape Memory Effect in NiTi Orthodontic Wires," *Journal de Physique IV*, Vol. C8, 1995, 1205–1210.

M. Ahmadian
Associate Editor